Design, Manufacturing and Applications of Composites

PROCEEDINGS OF THE

ELEVENTH JOINT CANADA-JAPAN WORKSHOP ON COMPOSITES

FIRST JOINT CANADA-JAPAN-VIETNAM WORKSHOP ON COMPOSITES

Ho Chi Minh, Vietnam

AUGUST 8-10, 2016

EDITED BY

Suong Van Hoa

Concordia University, Montreal, Canada

Hiroyuki Hamada

Kyoto Institute of Technology, Kyoto, Japan

Nguyen Dinh Duc

Vietnam National University-Hanoi, Hanoi, Vietnam

DEStech Publications, Inc.

Design, Manufacturing and Applications of Composites

DEStech Publications, Inc.
439 North Duke Street
Lancaster, Pennsylvania 17602 U.S.A.

Printed in the United States of America
10 9 8 7 6 5 4 3 2 1

Main entry under title:
Design, Manufacturing and Applications of Composites: Proceedings of the Eleventh Joint Canada-Japan Workshop on Composites/First Joint Canada-Japan-Vietnam Wokshop on Composites

A DEStech Publications book
Bibliography: p.
Includes index p. 421

ISBN No. 978-1-60595-326-7

Contents

BIOCOMPOSITES

CHARACTERIZATION AND TESTING

PHYSICAL PROPERTIES

Committees

Executive Committee
Suong V. Hoa (Co-Chair), Concordia University, Canada
Truong Vo Van, Concordia University, Canada
Anh Dung Ngo, Ecole de Technologie Superieure, Canada
Tan Xuan Pham, Ecole de Technologie Superieure, Canada
Hiroyuki Hamada (Co-Chair), Kyoto Institute of Technology, Japan
Asami Nakai, Gifu University, Japan
Goichi Ben, Nihon University, Japan
Yoshimichi Fujii, Kyoto Institute of Technology, Japan
Takahisa Ueda, Nippon Pillar Packing Co., Ltd., Japan
Nobuo Takeda, The University of Tokyo, Japan
Hiroshi Suemasu, Sophia University, Japan
Takkashi Nagase, Toyota Motor Asia Pacific Engineering and Manufacturing Co., Ltd (TMAP-EM), Japan
Yamabe Masashi, Kanazawa Institute of Technology, Japan
Takahira Aoki, The University of Tokyo, Japan
Yoshio Aoki, Nihon University, Japan
Akira Todoroki, Tokyo Institute of Technology, Japan
Tsutomu Nagaoka, Nagoya University, Japan
Phan Thanh Binh, National University, Vietnam
Huynh Dai Phu (Co-chair), Ho Chi Minh City University of Technology, Vietnam
Truong Chi Thanh, Can Tho University, Vietnam
Doan Van Hong Thien, Can Tho University, Vietnam

Organization Committee
Rajamohan Ganesan, Concordia University, Canada
Mehdi Hojjati, Concordia University, Canada
Manju Misra, University of Guelph, Canada
Tri Dung Ngo, Alberta Innovates, Canada
Jason Lo, Canmet Canada, Canada
Tomohiro Yokozeki, The University of Tokyo, Japan
Masahito Ueda, Nihon University, Japan
Kentaro Okuno, Daiwa Plastics, Japan

Toshikazu Uchida, Uchida Co., Ltd., Japan
Yasunari Kuratani, Kado Corporation, Japan
Ryosuke Matsuzaki, Tokyo University of Science, Japan
Takayuki Sakai, Tokushima University, Japan
Ryo Marui, Marui Textile Machinery Co., Ltd., Japan
Nanami Norimichi, Nihon University, Japan
Tetsusei Kurashiki, Osaka University, Japan
Yoji Okabe, The University of Tokyo, Japan
Tetsuo Kikuchi, Toyu Giken Co., Japan
Takashi Furukawa, Hishiken Co., Japan
Ryosuke Matsuzaki, Tokyo University of Science, Japan
Yasumasa Nakanishi, Mie University, Japan
Toshihide Sugahara, Maruhachi Co., Japan

Advisory Committee

Anoush Poursartip, University of British Columbia, Canada
Johanne Denault, National Research Council, Canada
Larry Lessard, McGill University, Canada
Cheung Poon, Ryerson University, Canada
Toru Morii, Shonan Instituti of Technology, Japan
Hiroshi Ito, Yamagata University, Japan
Masayuki Okoshi, Kyoto Institute of Technology, Japan
Tatsuro Kosaka, Kochi University of Technology, Japan
Tadashi Uozumi, Gifu University, Japan
Gen Sasaki, Hiroshima University, Japan
Nguyen Trong Giang, Ha Noi Polytechnical University, Vietnam
Dang Mau Chien, National University, Vietnam
Nguyen Nang Dinh, National University, Vietnam
Nguyen Dinh Duc, National University, Vietnam

Preface

The Canada Japan workshops on composites is series workshops held every two years in a city in Canada and in Japan, starting in 1996. In 2016, the Canada-Japan-Vietnam workshop on composites was held in Ho Chi Minh city in Vietnam, August 8–10, 2016. The objectives are to provide opportunities for interaction between Canadian, Japanese and Vietnamese scientists and engineers working on composites. The workshop aims to foster collaboration between scientists and engineers working in Composites in Canada, Japan and Vietnam, and to provide a forum for the exchange of information and experience in the three countries. The workshop consisted of technical presentations and visits to local companies.

More than 80 participants from the three countries have participated in to the workshop. Topics vary from Materials development, Manufacturing, Bio composites, Analysis techniques, Physical properties, Impact damages, and Applications. There is a good proportion of contributions from the scientists in Vietnam. They provide a snapshot of work on composites in Vietnam.

Proceedings Co-editors

Suong Van Hoa
Concordia University
Montreal, Canada

Hiroyuki Hamada
Kyoto Institute of Technology
Kyoto, Japan

Nguyen Dinh Duc
Vietnam National University-Hanoi
Hanoi, Vietnam

Material Development

Enhancement of Energy Conversion Efficiency in Organic Solar Cell Using Nanoparticles

Nguyen Dinh Duc[*,1], Nguyen Nang Dinh[1], Pham Duc Thang[1], Dang Dinh Long[1] and Nguyen Xuan Nguyen[2]

ABSTRACT

Doping nanomaterials such as the nanoparticles, nanorods, nanoprisms, etc. into composite organic solar cells (OSCs) have recently attracted considerable research interest to obtain higher energy conversion efficiency. Among them, doping of Ag, ZnO nanoparticles into photoactive layers of multilayered composite OSCs are proposed to enhance the photocurrent due to the localized surface plasmon resonance (LSPR) effect. The size as well as the geometry of these nanoparticles are the most important key factors to contribute to LSPR effect. In this work we have investigated the LSPR effects of Ag and ZnO nanoparticles on the photoactive layer in a regular structure of OSC as ITO/photo-active layer doped with nanoparticles/ buffer layer/Al. The photoactive layer such as P3HT:PCBM doping with nanoparticles can be modeled as the light absorbed medium in which its physics behavior is altered by LSPR. Changing the size of Ag and ZnO nanoparticles, i.e. the radius, in P3HT:PCBM active layers will tune their absorption spectrum. The mechanical properties of nanoparticles doping in OSC structures based on P3HT:PCBM will also be discussed.

KEYWORDS

Organic solar cells, energy conversion efficiency, Ag and ZnO nanoparticles.

INTRODUCTION

In the recent years, organic solar cell (OSC) based on polymer has attracted much interest of the research community due to its great promise as renewable sources. One has also expected OSC to become the next generation photovoltaics for its low-cost, flexible as well as light devices which can be realized at room temperature solution processing. High energy conversion efficiency, i.e. exceeding 11% [1, 2, 3, 4] has been achieved in the polymer-fullerence bulk heterojunction (BFBHJ) type of devices

[1]VNU- University of Engineering and Technology, 144 Xuan Thuy, Cau Giay, Hanoi, Vietnam
[2]VNU-University of Science -334 Nguyen Trai, Thanh Xuan, Hanoi, Vietnam
*Email: ducnd@vnu.edu.vn

which may quickly bring the commercialized products of OSC-BFBHJ into life. The major obstacle towards the power conversion efficiency is the trade off between two main physics mechanisms inside OSC: the light harvesting, i.e. the light absorption and the charge collections, i.e. collections of photogenerated excitons. As the result, the mobility of charge-carrier is low and the exiton diffusion length is reduced due to the hopping limit. As the result, the thickness of the active layer is small, typically around 200 nm. Having such a thin active layer, OSC has a poor absorption process although the rate of charge-carrier recommbination is low [5, 6]. In most OSC structures, P3HT:PCBM is frequently used as a promising active layer which is able to exhibit the theoretical current J_{sc} close to 20 mA.cm^{-2}, the experimental value still falls short in the range of 12-14 mA.cm^{-2}. Hence, the main solution lies on the way to improve the light absorption of the P3HT:PCBM active layer, i.e. enhancing the light trapping process. Interestingly, localized surface plasmon resonance effect of nanoparticles (NPs) have been proposed to enhance the light absorption in medium [7, 8, 9, 10]. This has opened the new door to develop the OSC based on polymer structures as well as to create a new pathway for a better power conversion. More interestingly, mechanical properties of OSC will be influenced significantly by doping with NPs, for example, the Young and Bulk modulus of the OSC structures are affected in the presence of NPs. Figure 1 illustrates the regular structure of OSC doping the NPs.

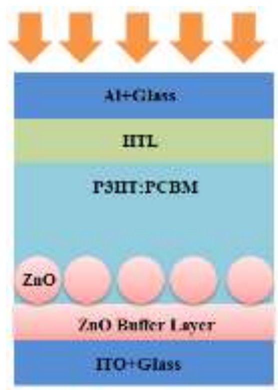

Figure 1. A regular structure of OSC, the NPs are illustrated with the spheres with the same radius. From top to bottom: incident light shining to Al+Glass electrode, the hole transport layer (HTL), P3HT:PCBM active layer, NPs in P3HT:PCBM are grown on top of ZnO buffer layer; ITO+Glass electrode.

The sections are organized as the follows: we will discuss the major role of NPs in enhancing the light traping process with LSPR in the next section. The numerical simulation using finite element technique will follow. The main findings will be discussed in the results and discussion section. And, the conclusion at the end will summarize our main findings.

LOCALIZED SURFACE PLASMON RESONANCE EFFECTS OF THE NANOPARTICLES

It is well-known that the metallic NPs, i.e. Au, Ag-NPs are scattered at the near field in the LSPR effect due the collective oscillations of electrons inside metal [8, 9, 10]. The similar calculation can be applied for the different type of non-metallic NPs, i.e. ZnO-NPs, nanorods, pyramids, so on. By using Mie theory [12, 13], the scattering and absorption cross section can be calculated as:

$$\sigma_{scat} = \frac{1}{6\pi}(\frac{2\pi}{\lambda})^4 |\alpha|^2, \quad \sigma_{abs} = \frac{2\pi}{\lambda}\mathrm{Im}[\alpha] \tag{1}$$

where, α is the polarized coefficient of NPs which reads:

$$\alpha = 3\Omega \frac{\varepsilon_P / \varepsilon_m - 1}{\varepsilon_P / \varepsilon_m + 2} \tag{2}$$

This quantity depends on the volumes of NPs, Ω, the dielectric of NPs ε_P, the dielectric of the surrounding environment ε_m. In case of $\varepsilon_p = -2\varepsilon_m$, the polarized coefficient of NPs diverges due to the LSPR effect. As the results, the cross section of LSPR NPs are much larger than the cross section of the typical NPs without LSPR. The larger the cross section is, the better light trapping process is. In other words, the harvesting light through the absorbance will be improved in the presence of LSPR and the power conversion efficiency will increase. As we may know, the NPs size has a large impact on the absorption spectrum. For example, the increase of the NPs size causes the red shift of the peaks in the spectrum. Moreover, the range of absorption spectrum is wider in the presence of LSPR effects. It can be explained by strong polarization occurred at the large effective NP size, i.e. the large cross sections. We should note that Mie scattering regime is only valid for the NPs with the diameters in the range of $0.1\lambda < d < 10\lambda$. In this work, we have chosen Ag for a case of the metallic nanoparticle instead of Au nanoparticle since Ag nanoparticle is cheaper than Au nanoparticle and there is not much different feature between their absorption spectrums. The diameter of Ag nanoparticle is about 100 nm and the diameter of ZnO-NPs is about 150 nm. These diameters are valid to apply the Mie theory.

NUMERICAL SIMULATION: FINITE ELEMENT METHOD

In this work, we will apply the finite element method (FEM) [14] for the different types of NPs which can be model as a perfect sphere. Comparing to other techniques, i.e. FDTD technique [15], FEM is a good choice for a complex problem since it will transform the continuos problem into the discrete one in a great manor. As a result, we have a good mesh which can be used to solve the PDEs and integral equations, i.e. the Maxwell's equations. In other words, we will map our problem into a set of the independent ordinary differential equations of the different smaller elements. We should note that a mapped mesh has to satify the following rules: firstly, the two different elements only share their boundaries. This condition will rule out the overlap between the two elements. The boundary can be the points, the lines as well as the surfaces. Secondly, the set of these elements forms a shape similar to the original one. In other words, the good grid can capture the most feature of the original system. This condition tries to avoid the empty space between the elements. An example of a FEM grid for a NP is illustrated in Figure 2 below.

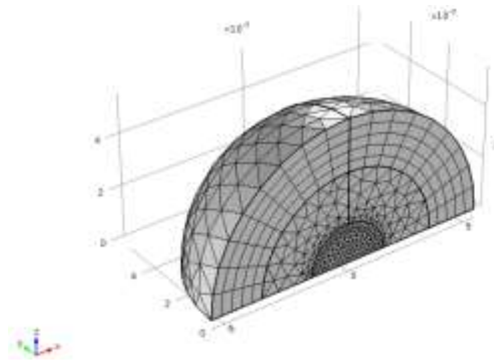

Figure 2. A typical quarter of NPs mesh using in a FEM simulation.

Figure 2 shows only a FEM mesh for a quarter of a nanoparticle since a particle is a perfect sphere with the high symmetry. There should not be any different between the full mesh for a sphere and its quarter but we will save the computing time as well as CPU memory by using a quarter of a NP instead of a full NP in FEM mesh. Following the standard way, we divide the original volume Ω into the different smaller volume elements Ω_s in which its size can be described by an unknown function $\phi \approx \sum_{i=1}^{N} f_i \rho_i$. Here, f_i is the basic polynomial functions and ρ_i is the coefficients. Due to the second rule stated above, the discrepency between the approximated functions and ϕ is close to zero as much as possible. The set of equations for the unknown coefficients are now ready to solve. We should note that the different elements are meshed following the first rule mentioned above. The boudary conditions of a different volume elements Ω_s and the approximated function ϕ are constrained and could be applied Neuman's condition $n.\nabla\phi = S$ or Dirichlet's condition $\phi = S$; where S is a scalar function and n is a normal vector to the boundary. In this manuscript, we will apply COMSOL multiphysics based on FEM technique to investigate the absorption spectrum of different NPs: Ag and ZnO NPs.

RESULTS AND DISCUSSION

We will start with ZnO nanoparticle, the radius is about 150 nm, doping into P3HT:PCBM active layer. In order to investigate the LSPR effect of ZnO nanoparticle, we will compare its absorption spectrum in two different environments: a pure air and P3HT:PCBM.

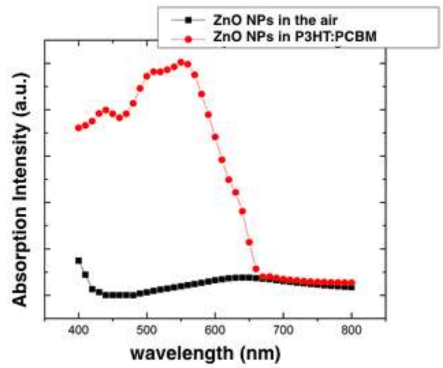

Figure 3. The absorption intensity of ZnO-NPs versus the wavelength in two environments: in air (black filled circles) and in P3HT:PCBM (red filled circles).

Figure 3 shows the absorption spectrum of ZnO-NPs in air (black filled circles) and ZnO-NPs in P3HT:PCBM (red filled circles). The two curves are obviously different: ZnO-NPs in air has a smooth curve and a weak peak in the infrared region whereas ZnO-NPs in P3HT:PCBM has a stronger peak around the two wavelengths $\lambda = 500nm$ and $\lambda = 580nm$. The higher absorption intensity in the wide range of invisible light has been observed as well. We conclude that the oxide ZnO-NPs do not absorb the invisible light in the air but ZnO-NPs has a strong absorption effect in P3HT:PCBM. This can be explained simply using the LSPR theory: exciting ZnO-NPs with the invisible light induces the multi-oscilations, on other hand this will lead to the defraction as well as the absorption of light. Moreover, P3HT:PCBM owns the $\pi - \pi$ bindings in its polymer chain which causes the stronger absorption. This makes P3HT:PCBM become a better absorption environment. The LSPR effects of ZnO-NPs in P3HT:PCBM could be illustrated through the distribution of the electromagnetic field at different weavelengths.

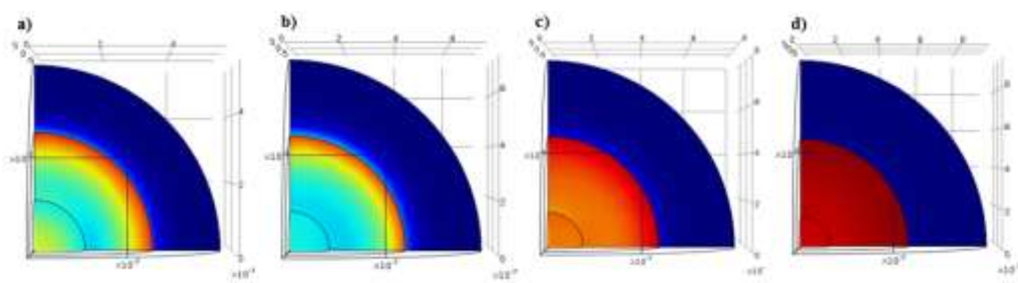

Figure 4. The distribution of the electromagnetic field of the ZnO-NPs in P3HT:PCBM with different incident wavelengths: a) λ =400 nm, b) λ =580 nm, c) λ =650 nm, d) λ =800 nm.

Figure 4 shows that the LSPR at the wavelengths $\lambda = 400nm$ and $\lambda = 580nm$ has stronger effects than LSPR in the infrared region, i.e. $\lambda = 650nm$ and $\lambda = 800nm$. As we can see, the red-shift of the incident light reduces the LSPR effect illustrated by the change of the electromagnetic field from $\lambda = 400nm$ to $\lambda = 800nm$. It also means that the defraction as well as the absorption of ZnO-NPs responses weakly to the incident light with a large wavelength, i.e. the infrared region.

More interesting, ZnO indeed has a strong LSPR effect although metallic NPs such as Au, Ag-NPs are previously well-known to enhance LSPR. We therefore investigate the absoprtion spectrum of Ag-NPs and compare it with ZnO-NPs to verify this conclusion. The result is shown in Figure 5, obviously, the ZnO-NPs peak as well as its absorption intensity are much stronger than those of Ag-NPs. This also suggests us to use ZnO-NPs doping into OSC structure for a better the power conversion efficiency.

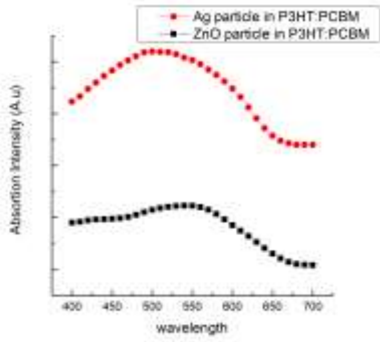

Figure 5. The absorption spectrum of Ag-NP (filled black square) and ZnO-NP (filled red circle).

Using Mie theory, it is easy to show that the larger the ZnO-NPs is, the further the absorption peak shifts to the near infrared region. We here also have recaptured this conclusion for ZnO-NPs in P3HT:PCBM with different NPs radius and the fixed incident light wavelength $\lambda = 580nm$.

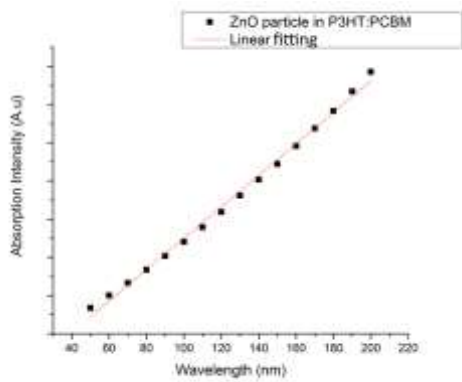

Figure 6. The dependence of absorption intensity on the radius of ZnO-NPs in P3HT:PCBM at the fixed wavelength λ =580 nm.

Figure 6 displays the dependence of the absorption intensity as a function of the radius of ZnO-NPs in P3HT:PCBM. From Mie theory, the scattering and absorption cross section is proportional to the dielectric function of NP, ε_p as written in Equation (2). In the rough approximation, i.e. using the simple Drude model, the dielectric function: $\varepsilon_p = 1 - \frac{\omega_p{}^2 e^2}{(\omega^2 + i\gamma\omega)}$ with ω_p is Plasma frequency, e is electron unit and e = 1.6 x 10^{-19} C, ω is frequency of the incident light. The absorption intensity is proportional to 1/r as the follows: $\gamma(r) = \gamma_0 + \frac{Av_f}{r}$, with v_f is electron velocity at Fermi level. Hence, the absorption cross sections σ_{abs} is quantitatively proportional to the radius r which is well consistent with Mie theory. This result is important since one is able to control the absorption and scattering properties of NPs by tuning the radius of NPs.

MECHANICAL EFFECT OF NANOPARTICLES ON OSC COMPOSITE STRUCTURE

The role of particles in several FGM structures at macroscopic scale is well known. However, the role of particles in the multilayered structure at nano-scale has not been known much. Other than the enhancement of the energy conversion, the nanoparticle can stabilize the OSC multilayered structure. Therefore, it should be interesting to take a closer look at the mechanical properties of these NPs in our structure of interest. We can use a simple model to investigate this problem as the following: the NPs are considered as the ideal spheres with the same radius r (nm). The elastic, homogeneous and isotropic conditions for NPs are assumed. Under these conditions, the most two important parameters, which we should take into account, are Young's (E) and bulk (K) modules. At nano-scale, the mechanical coupling between the different ingredients can be represented by the stress distribution as the follows:

$$\sigma_{ik} = \sigma_{ik}^{0} + \sigma_{ik}^{(1)} + \sigma_{ik}^{(2)} + \ldots \quad (3)$$

Where, σ_{ik}^{0} is the homogeneous stress, $\sigma_{ik}^{(1)}$ is coupling stress between matrix and particles, $\sigma_{ik}^{(2)}$ is the coupling stress between the nearest particles. We will cut off the stress distribution at the first order of coupling, meaning we only take into account the first and the second term in Equation (3), for the simplicity. We, now, are able to apply the well-known Lame's equilibrium equation for the displacement components *u* as the follows:

$$2(1-v)\nabla\nabla.\bar{u} - (1-2v)\nabla\times\nabla\times\bar{u} = 0 \quad (4)$$

The mechanical effects can be extracted by solving the Equation (4) under the additional assumption in which the location of stress for NPs at nano-scale is at the center of the particles [16]. As the results, we can obtain that the dispersion of NPs doping in polymers structure such as P3HT:PCBM have increased both the effective Young's (E_{eff}) and effective bulk modulus (K_{eff}). This finding is similar to our finding of TiO_2 doping in MEH-PPV-OSC structure. In other words, the NPs not only enhance the energy conversion but also increase the stability as well as lifetime of the OSC multilayered structure. This conclusion is important for the commercial products.

CONCLUSION

In this manscript, we have investigated the effects of the metallic nanoparticle Ag and non-metallic nanoparticle ZnO on the power conversion efficiency as well as the mechnical impact on the OSC devices. We have found that the absorption of ZnO is enhanced inside P3HT:PCBM environment due to LSPR. In other words, the harvesting light process in active layer has been affected by using ZnO-NPs. We have also found a similar behavior for Ag-NPs except the weaker absoprtion intensity and the peak. The mechanical properties of OSC devices such as the effective Young's and effective bulk modulus doping with ZnO-NPs and Ag-NPs have been improved.

ACKNOWLEDGEMENTS

This work has been supported by Vietnam National University, Hanoi (VNU), under Project No. **QG.15.24.**

REFERENCES

1. C.-C. Chen, W.-H. Chang, K. Yoshimura, K. Ohya, J. You, J. Gao, Z. Hong, and Y. Yang. 2014, "*An Efficient Triple-Junction Polymer Solar Cell Having a Power Conversion Efficiency Exceeding 11%,*" Adv. Mat., 26: 5670-5677.
2. Li, G., Zhu, R. & Yang, Y. 2012, "*Polymer solar cells*," Nature Photon., 6: 153-161.
3. Li, Y. F. 2012, "*Molecular design of photovoltaic materials for polymer solar cells: toward suitable electronic energy levels and broad absorption*," Acc. Chem. Res., 45: 723-733.
4. You, J. et al. 2013, "*A polymer tandem solar cell with 10.6% power conversion efficiency*," Nature Commun., 4: 1446.
5. V. Shrotriya, et al. 2014, "*Efficient light harvesting in multiple-device stacked structure for polymer solar cells* ," Appl. Phys. Lett. 88: 064104.
6. G. Dennler, et al. 2009, "*Polymer-Fullerene Bulk-Heterojunction Solar Cells*," Adv. Mater. 21: 1323.
7. Morfa AJ, Rowlen KL, Reilly III TH, Romero MJ, Van de Lagemaat J. 2008, "*Plasmon-enhanced solar energy conversion in organic bulk heterojunction photovoltaics*," Appl. Phys. Lett. 92:013504.
8. Rand BP, Peumans P, Forrest SR. 2004, "*Long-range absorption enhancement in organic tandem thin-film solar cells containing silver nanoclusters*," J. Appl. Phys. 96:7519-26.
9. Kim K, Carroll DL. 2005, "*Roles of Au and Ag nanoparticles in efficiency enhancement of poly(3-octylthiophene)/C-60 bulk heterojunction photovoltaic devices*" Appl. Phys. Lett. 87:203113.
10. S. Linic, P. Christopher, and D. B. Ingram. 2011, "*Plasmonic-Metal Nanostructures for Efficient Conversion of Solar to Chemical Energy*," Nat. Mater., 10 (12): 911-921.
11. E. Stratakis and E. Kymakis. 2013, "*Nanoparticle-based plasmonic organic photovoltaic devices*," Mater. Today 16(4), 133-146.
12. Mie, G. 1908, "*Beiträge zur Optik trüber Medien, speziell kolloidaler Metallösungen*," Annalen der Physik 330 (3): 377-445.
13. Michael Quinten, "*Optical properties of nanoparticle systems: Mie and beyond*", Wiley-VCH, 2011, pp. 76-101,170.
14. P. Monk. 2003, "*Finite element methods for Maxwell's equations*", Oxford University Press
15. Atef Elsherbeni and Veysel D. 2009, "*The Finite Difference Time Domain Method for Electromagnetics with MATLAB Simulations*", SciTech Publishing.
16. Chung D. N., Dinh N. D., David H., Duc N. D., Trung T. Q and Mircea C. 2013, "*Investigation of polymeric composite films using modified TiO2 nanoparticles for organic light emitting diodes*", Current Nanoscience. 9 (1): 14-20.

Design Model for Hybrid Steel-RC Walls

Quang-Huy Nguyen[1], Van Toan Tran[2] and Mohammed Hjiaj[1]

ABSTRACT

Hybrid RCS frames consisting of reinforced concrete (RC) column and steel (S) are used frequently in practice for mid to high-rise buildings. RCS frames possess several advantages from structural, economical and construction view points compared to either traditional RC or steel frames. One of the key elements in RCS frames is the composite shear wall consisting of several steel sections encased in reinforced concrete. Regarding the RC walls reinforced by more than one steel profile, namely "Hybrid" wall, although a number of researchers have focused on its various aspects, they are currently not covered by standards because they are neither reinforced concrete structures in the sense of Eurocode 2 or ACI318, nor composite steel-concrete structures in the sense of Eurocode 4 or AISC 2010. This paper is dedicated to present a tentative design model for hybrid walls with several embedded steel profiles subjected to combined axial force, bending and shear. The model is based principally on the design rules of Eurocode 2 and Eurocode 4. Particular attention will be paid to shear (longitudinal and transversal) resistances because preventing shear failure is one of the major concerns when designing a composite structural member. A strut-and-tie model is developed to evaluate the transverse shear resistance taking into account the contribution of the steel profiles. Furthermore, an analytical method is proposed for the prediction of the longitudinal shear stress at the concrete-steel profile interface which allows to design adequate shear connection of the profile to concrete. The proposed design model provides a faire estimation of the part of applied shear which is applied to the embedded steel profiles; this allows to take into account the influence of transverse shear on the combined axial force and bending resistance. When used with design values of bond and friction shear strength of Eurocode 4, the proposed design model gives a faire estimation of the longitudinal shear stress at the concrete-steel profile interface.

Keywords: Steel-concrete hybrid shear walls, shear connection, design method, static test.

[1]National Institute of Applied Sciences Rennes, Dept. Civil Engineering and Urban, France
[2]Thuyloi University, Vietnam

INTRODUCTION

Nowadays, hybrid reinforced concrete steel (RCS) frames consisting of reinforced concrete (RC) column and steel (S) are used frequently in practice for mid to high-rise buildings. RCS frames possess several advantages from structural, economical and construction view points compared to either traditional RC or steel frames. As described by Griffis (Griffis, 1986), RCS frames effectively combine structural steel and reinforced concrete members to their best advantage. From construction view point, these systems are usually built by first erecting a steel skeleton, which allows the performance of different construction tasks along the height of the building. One of the key elements of RCS frames is the steel-concrete composite core wall, where the practice of encasing structural steel shapes encased in reinforced concrete is common. For many years, the traditionally reinforced concrete shear walls have been used as the primary lateral load resisting system in multistory buildings. Although reinforced concrete shear walls have many structural and economical advantages some disadvantages appear when using this structural system in buildings subjected to seismic action. One of the main disadvantages is the development of tension cracks in tension zones and compressive crushing in localized compression areas during large cyclic excursions. Such cracks and crushing failures can result in splitting and spalling failure of the wall with serious deterioration of stiffness and reduction in strength. Steel-concrete composite shear walls can mitigate most disadvantages of RC shear walls and take advantage of the best characteristics the RC and the steel can offer.

Various types of composite walls have been developed, investigated and used for core walls of high-rise buildings in seismic zones. Zhao and Astaneh-Asl (Zhao, 2004) attached RC panels to the steel plate walls using bolts, resulting in highly ductile behavior and stable cyclic post-yielding performance. Saari et al. (Saari, 2004) studied the behavior of headed shear stud connectors for use in steel frames with partially restrained connections and reinforced concrete infill walls, attached compositely to the steel frame around the perimeter of each wall panel. They pointed out that, in infill walls, the shear connectors lie in the plane of the concrete panel, which results in different behavior from studs in composite beams. Experimental results shown that the presence of axial tension greatly reduced the stud shear strength and deformation capacity when no confining reinforcement was provided. When confining reinforcement was provided, test results correlated better with existing design equations. Tong et al. (Tong, 2005) conducted an experimental study of the cyclic behavior of a composite structural system consisting of partially-restrained steel frames with reinforced concrete infill walls. The composite interaction is achieved through the use of the headed stud connectors along the steel frame-infill interfaces so that the two main components of the system share in the resistance of lateral shear and overturning moment. They concluded that this system has the potential to offer strength appropriate for resisting the forces from earthquakes and stiffness adequate for controlling drift for low to moderate-rise buildings located in earthquake-prone regions. Zhou et al. (Zhou Y. X., 2010) performed experimental and numerical studies of composite shear with multi-embedded steel sections at wall boundaries as well as wall middles. They indicated that composite shear walls with multi-embedded steel sections had better energy dissipation capacity than that with steel sections only at boundaries. The presence of multi-embedded steel sections did not affect the final failure mode of the composite shear walls, but they would restrain the development of cracks and prevent the concrete from serious spalling. Similar kind of composite shear walls was experimentally and numerically studied by Dan et al. (Dan, 2011). They encased vertical steel profiles into RC walls and demonstrated the effectiveness of the steel profiles in improving the seismic performance of RC shear walls. Qian et al. (Qian, 2012) investigated the behavior of composite shear walls with embedded steel tubes at the wall boundaries and proved that such composite details can ensure good seismic performance under high axial load and cyclic lateral loading. Rafiei et al. (Rafiei, 2015); Hossain et al. (Hossain, 2016) studied the behavior of composite shear walls consisting of two skins of profiled steel sheeting and an infill of concrete under in-plane monotonic and cyclic loading respectively, demonstrating more ductile behavior and higher energy absorbing capacity. Chen et al. (Chen, 2015) investigated the double steel plate-high strength concrete composite walls with concrete filled steel tube boundary elements, showing high strength and excellent deformation capacity. Wu et al. (Wu, 2016) studied the seismic behavior of steel and concrete composite shear walls with embedded steel truss. Test results indicated that the embedded truss web braces affect significantly the hysteretic behavior of the composite walls in terms of lateral load capacity, energy dissipation and ductility, while the embedded truss chords can enhance the lateral load capacity. Zhang et al. (Zhang, 2016) proposed and investigated a new structural shear wall consisting of bundled lipped channels seam-welded together and in-filled concrete. They pointed out that that the level of axial force ratio and the configuration detail significantly affect the entire hysteresis performance, while the presence of shear studs delays the occurrence of fracture and failure.

Regarding the RC walls reinforced by more than one steel profile, namely hybrid wall, although a number of researchers have focused on its various aspects, they are currently not covered by standards because they are neither reinforced concrete structures in the sense of Eurocode 2 (Eurocode 2, 2004) or ACI-318 (ACI-318, 2005), nor composite steel-concrete structures in the sense of Eurocode 4 (Eurocode 4, 2004) or AISC (ANSI/AISC 360-05, 2010). Gaps in knowledge are mostly related to the problem of force transfer between concrete and embedded steel profiles, a situation in which it is neither known how to combine the resistances provided by bond, by stud connectors and by plate bearings, nor how to reinforce the transition zones between classical reinforced concrete and concrete reinforced by steel profiles. This paper is dedicated to present a tentative design model for hybrid walls with several embedded steel profiles subjected to combined axial force, bending and shear. This model is based principally on the design rules of Eurocode 2 (Eurocode 2, 2004) and Eurocode 4 (Eurocode 4, 2004). Particular attention will be paid to shear (longitudinal and transversal) resistances because preventing shear failure is one of the major concerns when designing a composite structural member. Experiments conducted with steel-concrete composite columns (simple encased steel profile) shown that the shear failure generally involves two possible failure modes: (1) the diagonal shear failure, which closely resembles the shear failure of an ordinary reinforced concrete structural member; and (2) the shear bond failure, which results in cracks along the interface of the steel profile and concrete. For this reason, a strut-and-tie model is developed to evaluate the transverse shear resistance taking into account the contribution of the steel profiles. Furthermore, a analytical method is proposed for the prediction of the longitudinal shear stress at the concrete-steel profile interface which allows to design adequate shear connection of the profile to concrete. Finally, a hybrid wall with three steel profiles is designed using the proposed method and the design resistance values are compared to the ones obtained by an Abaqus FE model.

DESIGN MODEL

As already mentioned in the introduction, the studied hybrid walls are not yet covered by design standards. The present study aims to develop a tentative design method for such element subjected to combined axial force, bending and shear. Let consider a hybrid steel-concrete element subjected to axial force, bending and shear as shown in Figure 1. The cross-section consists of a rectangular RC section reinforced by several steel profiles. Question can be raised as how to assess the strength of this type of section. Can we simply consider it as reinforced concrete section in sense of Eurocode 2 (Eurocode 2, 2004) or ACI-318 (ACI-318, 2005) and apply them for design or as composite steel-concrete section in sense of Eurocode 4 (Eurocode 4, 2004) or AISC (ANSI/AISC 360-05, 2010). For this kind of composite element, gaps in knowledge are mostly related to the problem of force transfer between concrete and embedded steel profiles. In the case where the full interaction between steel profiles and concrete is ensured (by bond and/or connectors such as shear studs or plate bearings), the steel profiles can be considered as reinforcement rebars their bending and shear resistances can be evaluated using reinforced concrete standards. Otherwise, for the bending resistance the concept of composite section of Eurocode 4 (Eurocode 4, 2004) or AISC (ANSI/AISC 360-05, 2010) can be also used however the shear resistance of the composite section built-up from two or more encased steel is not yet covered by these standards.

In the proposed design method, particular attention will be paid to shear (longitudinal and transversal) resistances because preventing shear failure is one of the major concerns when designing a such composite structural member. Experiments conducted with simple encased steel profile shown that the shear failure generally involves three possible failure modes:

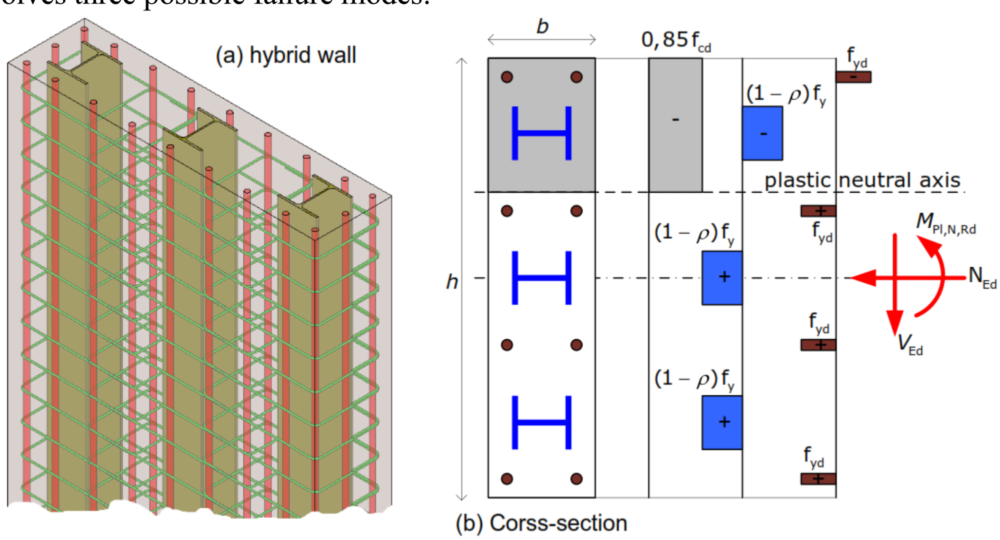

Figure 1. Description of studied hybrid walls

(1) the diagonal shear failure, which closely resembles the shear failure of an ordinary reinforced concrete structural member;

(2) the longitudinal shear failure, which results in cracks along the interface of the steel flange and concrete.

(3) the flexural failure, which results in vertical cracks at mid-span.

A method for the calculation of the number of connector to ensure the full interaction between steel profiles and concrete around is firstly developed. The bending resistance will be determined using the M-N interaction curve which is build using the method of stress distribution of Eurocode 4 (Eurocode 4, 2004). Regarding the shear resistance, a strut-and-tie model is developed taking into account the contribution of the steel profiles. For the sake of simplicity, in this work, we consider only the case of three encased steel profiles. The three steel profiles are oriented such that they are submitted to weak axis bending. It is assumed that the second order effect is negligible.

DESIGN RESISTANCE OF CROSS-SECTION TO COMBINED COMPRESSION AND BENDING

There is nowadays no design standard providing the guidance on how to determine properly the plastic resistances of composite section with more than one encased steel profile. However, once the steel profiles are fully embedded in concrete, the resistance of hybrid cross-sections to combined compression and bending and the corresponding interaction curve may be calculated assuming rectangular stress blocks as shown in Figure 1. This method is inspired from the simplified method of design of Eurocode 4 (Eurocode 4, 2004). In this method, the tensile strength of the concrete is neglected.

If the shear force $V_{a,Ed}$ acting on one steel section exceeds 50% of the design shear resistance of the steel section $V_{pl,a,Rd}$ (see EC3-1-1§6.2.6(2)) (Eurocode 3, 2004), the influence of the transverse shear on the resistance in combined bending and compression should be taken into account by a reduced design steel strength $(1\text{-}\rho)f_y$ where:

$$\rho = \left(\frac{2V_{a,Ed}}{V_{pl,a,Rd}} - 1 \right)^2 \tag{1}$$

The shear force $V_{a,Ed}$ acting on one steel section is assumed to be determined by:

$$V_{a,Ed} = \frac{V_{Ed}}{n_a} \frac{M_{pl,a,Rd}}{M_{pl,Rd}} \tag{2}$$

where $M_{pl,a,Rd}$ is the plastic resistance moment of n_a steel sections and $M_{pl,Rd}$ is the plastic resistance moment of the hybrid section.

DESIGN TRANSVERSE SHEAR RESISTANCE

If the encased steel profiles are considered as reinforcing bars, the shear resistance can be evaluated using the strut-and-tie model proposed in Eurocode 2 (Eurocode 2, 2004). However it is obvious that the shear resistance provided by the steel profiles must be not negligible for such hybrid section. In our design approach it is assumed that the shear resistance of the hybrid section is given by adding up the shear resistances of RC section and composite steel-concrete section. As shown in Figure 2, the composite section has a width limited to the width of the steel shape h_a and the RC section has a width b_c=b- h_a where b being the width of hybrid section.

$$V_{Rd} = V_{Rd,RC} + V_{Rd,a} \tag{3}$$

where:

- $R_{d,RC}$ is the design shear resistance of RC section which is determined in accordance with EN 1992-1-1 §6.2.3(3):

$$V_{Rd,RC} = \min \left| \begin{aligned} V_{Rd,s} &= \frac{A_{sw}}{s} z f_{ywd} \cot\theta \\ V_{Rd,max} &= \frac{\alpha_{cw} b_c z \upsilon_1 f_c}{\cot\theta + \tan\theta} \end{aligned} \right| \tag{4}$$

- $V_{Rd,a}$ is the design shear resistance of composite section which is given by:

$$V_{Rd,a} = n_a (1-\eta) V_{pl,a,Rd} \tag{5}$$

with n_a being the number of steel profiles; $V_{pl,a,Ed}$ being the design shear resistance of one steel section determined in accordance with EN 1993-1-1§6.2.6(2); The coefficient η represents the influence of normal stress on the shear resistance of steel profile when the design axial force exceeds *50%* of the plastic resistance to compression $N_{pl,Rd}$:

$$\eta = \left(\frac{2N_{Ed}}{N_{pl,Rd}} - 1 \right)^2 \tag{6}$$

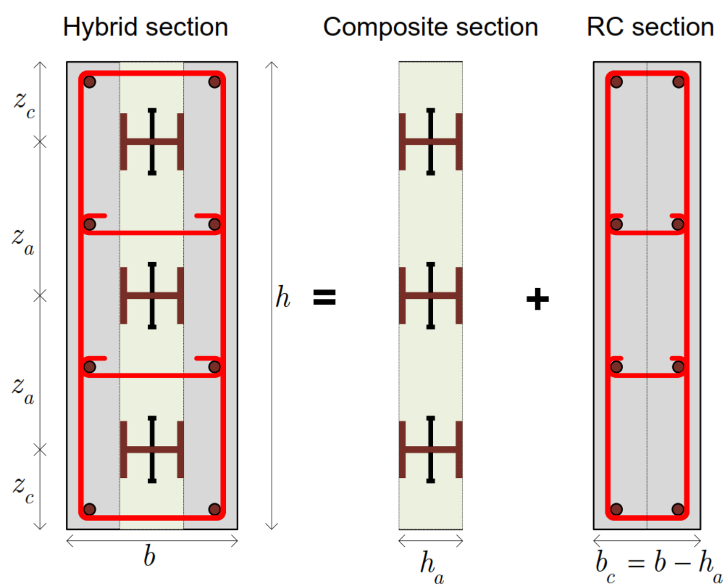

Figure 2. Decomposition of hybrid section into a RC section and composite section

DESIGN LONGITUDINAL SHEAR RESISTANCE

Vertical force equilibrium:

$$V_{Ed} = bz\sigma_{cw}\sin^2\theta + n_a V_{a,Ed} \tag{7}$$

where σ_{cw} is the compression stress in struts; z is the distance between the compression and tension chords. In wall with huge embedded steel sections, it is proposed to consider z as the distance between the center of top and bottom embedded profiles. θ is the inclination of the compression struts.

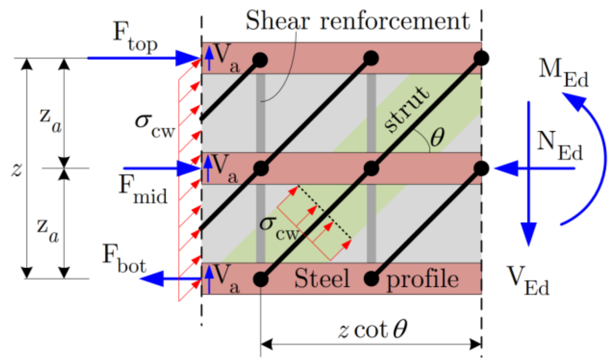

Figure 3. Strut-and-tie model fore shear force transfer in hybrid wall

The longitudinal shear force acting on the bottom (or top) embedded profile can be obtained by:

$$g_{Ed} = \frac{h_a\sigma_{cw}(\cos\theta - \mu\sin\theta)}{z_a\cot\theta} \tag{8}$$

If the longitudinal shear force g_{Ed} is greater than the design shear strength τ_{Rd} given in Eurocode 4 (Eurocode 4, 2004), shear connectors are therefore needed to ensure the full interaction between steel profiles and concrete. In this case, the longitudinal shear force, namely V_L, acting on the shear connectors from the cross-section where the full plastic bending moment is reached to the cross-section where the bending moment vanishes is:

$$V_L = A_a(1-\rho)f_y \tag{9}$$

where A_a is area of one steel profile. The minimum number of shear stud needed for one steel profile to ensure the full interaction is $n_{min}=V_L/P_{Rd}$ where P_{Rd} is design shear resistance of one shear connector.

NUMERICAL APPLICATION

The proposed design model is now used to evaluate the resistance to combined bending and shear of a composite wall reinforced by three encased steel profile. The geometric and material characteristics are presented in Figure 4.

The prediction of the longitudinal shear stress at concrete-steel profile interface is presented in *Table I*. As can be seen, at the maximum applied load the predicted shear stress g_{Ed} is greater than the design shear strength τ_{Rd} which is taken equal to 0.51 MPa according to Eurocode 4 part 1 §6.7.4.3(4). This points out that in all specimens for design conditions the shear connectors are always requited to provide at least a shear resistance equal to 0.51 MPa.

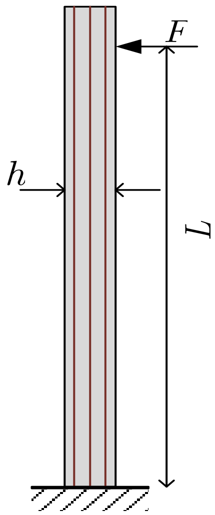

Specimen	Steel profile	Rebar	Stirrups and pins	Stirrup spacing (mm)	Connector	Connector spacing (mm)
BW	3HEB100	8HA20	HA16	200		
CW	3HEB100	8HA20	HA16	200	40 Nelson H3L16mm	200

- Distance between two axes of supports: L=1875mm;
- Design concrete resistance: $f_c = f_{ck}$=30MPa;
- Steel profile resistance: f_y=460MPa (S460);
- Steel rebar resistance: f_{yk}=500MPa;
- Dimensions of the cross-section: height h=900mm and width b=250mm.

Figure 4. The geometric and material characteristics of hybrid wall

TABLE I. SAMMERY OF DESIGN RESISTANCE

Design calculation						EC4
Specimen	$V_{a,Ed}$ (kN)	σ_{cw} (MPa)	$^{*}g_{Ed}$ (MPa)	$M_{pl,Rd}$ (kNm)	V_{Rd} (kN)	$^{**}\tau_{Rd}$ (MPa)
BW	130	5.96	0.75	1446	1614	0.51
CW	131	6.39	0.81	1493	1614	

* *the coefficient of friction is taken as 0.5 (see Eurocode 4 part 1 §6.7.4.2(4))*

** *τ_{Rd} including β factor of Eurocode 4 for concrete cover greater than 40mm; β=1.7*

CALIBRATION OF PROPOSED DESIGN MODEL BY NUMERICAL 3D MODEL

The proposed design model is now calibrated by a numerical 3D model. The hybrid wall considered in the previous section is now simulated by Abaqus FE software where solid elements are adopted for concrete, steel profiles and connectors and truss elements are used for steel reinforcement. Regarding the material models, concrete damaged plasticity model is used. The model parameters are selected to provide more or less the same stress-strain curve for uniaxial compression given in Eurocode 2. In this numerical model, steel reinforcement is embedded in concrete while "Hard contact" and "Frictionless" interactions are used to connect steel profiles and shear stud to concrete around. Figure 5 and Figure 6 show the load-displacement curve obtained by the numerical model. The design-numerical comparison of the shear force in steel profiles is presented in Table I and Figure 6. As can be seen, the design value is quiet well calibrated by the numerical results.

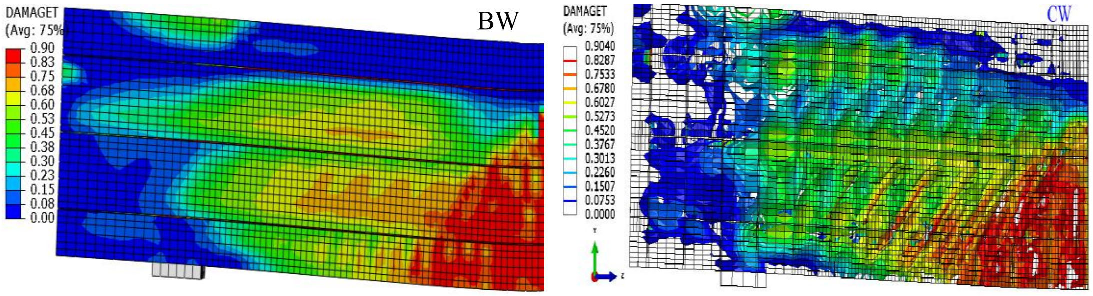

Figure 5. Crack distribution in the concrete at defection level of 60mm

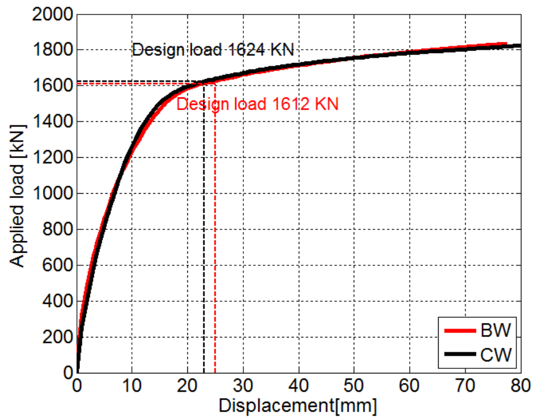

Figure 6. Numerical results

CONCLUSIONS

In this paper, a design model for hybrid walls subjected to combined compression, bending and shear has been proposed. Particular attention has been paid to transverse shear resistance for which a strut-and-tie model has been developed taking into account the contribution of the steel profiles. Furthermore, the proposed design model provides a method to evaluate longitudinal shear the concrete-steel profile interface, which is necessary to design an adequate shear connection of the profile to concrete.

REFERENCES

ACI-318. (2005). Building code requirements for reinforced concrete. *American Concrete Institute*.

ANSI/AISC 360-05. (2010). *Specifications for Structural Steel Buildings.* American Institute for Steel Construction.

Chen, L. H.-M. (2015). Seismic behavior of double steel plate-HSC composite walls. *Engineering Structures, 102*, 1-12.

Dan, D. A. (2011). Theoretical and experimental study on composite steel-concrete shear walls with vertical steel encased profiles. *Journal of Constructional Steel Research, 67*(5), 800-813.

Echigo, S. Y. (1998). New type hybrid structure and practical analysis method of creep and shrinkage. *Construction and Building Materials, 12*(2-3), 93-103.

Eurocode 2. (2004). *EN1992-1-1 Design of concrete structures-Part 1: General rules and rules for buidings.* European Standards - European Commission.

Eurocode 3. (2004). *Design of concrete structures. Part 1: General rules and rules for buidings.* European Standards - European Commission.

Eurocode 4. (2004). *EN1994-1-1 Design of composite steel and concrete structures-Part 1: General rules and rules for buildings.* European Standards - European Commission.

Griffis, L. (1986). Some design considerations for composite-frame structures. *Engineering Journal, 23*(2), 59-64.

Hossain, K. S. (2016). Structural performance of profiled composite wall under in-plane cyclic loading. *Engineering Structures, 110*, 88-104.

Morino, S. (1998). Recent developments in hybrid structures in Japan-research, design and construction. *Engineering Structures, 20*(4-6), 336-346.

Qian, J. Z. (2012). Behavior of steel tube-reinforced concrete composite walls subjected to high axial force and cyclic loading. *Engineering Structures, 36*, 173-184.

Rafiei, S. K. (2015). Profiled sandwich composite wall with high performance concrete subjected to monotonic shear. *Journal of Constructional Steel Research, 107*, 124-136.

Saari, W. J. (2004). Behavior of shear studs in steel frames with reinforced concrete infill walls. *Journal of Constructional Steel Research, 60*(10), 1453-1480.

Tong, X. J. (2005). Cyclic behavior of steel frame structures with composite reinforced concrete infill walls and partially-restrained connections. *Journal of Constructional Steel Research, 61*(4), 531-552.

Wu, Y. D. (2016). Seismic performance of steel and concrete composite shear walls with embedded steel truss for use in high-rise buildings. *Engineering Structures, 125*, 39-53.

Zhang, X. Y. (2016). Experimental seismic behavior of innovative composite shear walls. *Journal of Constructional Steel Research, 116*, 218-232.

Zhao, Q. a.-A. (2004). Cyclic Behavior of Traditional and Innovative Composite Shear Walls. *Journal of Structural Engineering, 130*(2), 271-284.

Zhou, Y. X. (2010). Seismic behavior of composite shear walls with multi-embedded steel sections. Part II: analysis. *The Structural Design of Tall and Special Buildings, 19*(6), 637-655.

Zhou, Y. X. (2010). Seismic behaviour of composite shear walls with multi-embedded steel sections. Part I: experiment. *The Structural Design of Tall and Special Buildings, 19*(6), 618-636.

Author Index